

## PERFORMANCE EVALUATION OF A MICRO GAS TURBINE BASED ON AUTOMOTIVE TURBOCHARGER FUELLED WITH LPG

**Guenther Carlos Krieger Filho, guenther@usp.br**

**José Rigoni Junior**

**Rafael Cavalcanti de Souza, rafael.cavalcanti.souza@gmail.com**

Laboratory of Environmental and Thermal Engineering (LETE)

Department of Mechanical Engineering (PME)

Escola Politécnica da Universidade de São Paulo (EPUSP)

Cidade Universitária - São Paulo – SP – CEP 055809-900

**Abstract.** *This work is concerned with the design and experimental evaluation of a low cost microgasturbine. Alternative electricity is needed due to the high energy demand nowadays. From the many solutions available, gas turbines associated to electric generator is on the solutions analyzed by many research centers in many universities. In the present work, a low cost solution is based on an automotive turbocharger unit coupled to a combustion chamber and electric generator. In present work, the gas turbine cycle was thermodynamically analyzed and the combustion chamber geometry was simulated with the finite volume method. Some aspects of design process of the combustion chamber and power turbine rotor are discussed. Experimental data of pressure and temperature were measured at the combustion chamber inlet and outlet positions. The mass flow in steady regime was 0.17 kg/s and the turbine inlet temperature 750°C. Under these operating conditions, the fuel consumption rate of LPG is 0.0028 kg/s. The net power, measured at the output shaft range between 1 and 1,5kW, depending on rotation. Besides experimental data, a comparison is done between CFD design of the combustion chamber and the measured outlet temperature. The numerical results of the temperature and velocity field inside the combustor are presented. Also the bluff body flame stabilization is discussed.*

**Keywords:** *micro gas turbine, combustion chamber CFD, power turbine.*

### 1. INTRODUCTION

The use of micro-gas turbine in cogeneration systems increases continuously. Micro gas turbines emerged as a viable solution because of its high power density and efficiency, when compared to similar thermal machines. Diesel engines are also used for local power generation, but gas turbines have advantages over these types of machine due to the already mentioned characteristics, plus the high power/weight density. It's estimated that large gas turbines have a power to weight ratio over 25 times that of diesel engines. But gas turbines are more sensitive to fuel quality and also are more expensive due to the use of high technology engineering and materials (Wilson et al, 1998).

A low cost micro gas turbine was developed using an automotive turbocharger for research purposes. In order to obtain useful shaft power, a free power turbine was developed and connected to an electric generator via gearbox.

This paper deals with numerical simulation of combustion chamber and experimental evaluation of a micro gas turbine based on automotive turbocharger. Also, it's shown how the basic design of the free power turbine was carried out.

### 2. EXPERIMENTAL SETUP

The micro gas turbine proposed in this work can be divided into three major components: combustion chamber, automotive turbo charger and power turbine unit. The use of an automotive turbocharger was due to the quick availability of such component, allowing the designers to focus their attention to the combustion chamber and the power turbine. In the next sessions, the design of these two components is discussed in more detail. This session deals with the experimental setup used to evaluate the performance of the micro gas turbine.

As mentioned before, the micro gas turbine is composed of three major components. These can be divided into two groups: gas generator, which comprises the combustion chamber and automotive turbocharger, and the power turbine, composed by the power turbine, gear box and electric generator.

A sketch of the experimental rig is shown in Figure 1. The combustion chamber (3) is positioned just over the turbine (4) inlet. The combustor receives air from the compressor (2) in a reverse flow concept. The air flow mass rate is measured using a calibrated ASME nozzle (1). The fuel mass flow rate is measured by means of rotameter (5), calibrated for LPG, or liquefied petroleum gas. The pressure at the compressor outlet is measured with the help of a manometer (6) while gas temperature at the combustion chamber outlet is measured with K-thermocouple (7) located at the centre of the exit plane. At the turbine outlet, temperature is measured with the N-thermocouple (8) and the flue gases composition (CO and O<sub>2</sub>) are measured with a gas analyzer TESTO ® 370-2 type. These components are part of the gas generator.

The power turbine (9) is fed with exhaust gas from the gas generator. This component is responsible for the usable power, generated in the micro gas turbine. The turbocharger unit operates at high speeds (around 100.000 rpm), and this made impossible to directly connect the electric generator to this component. The power turbine operates at speeds up to 15.000 rpm and it is connected to a gear box (10), which has a gear ratio of 4:1. The electric generator (11) can generate up to 2kW at 3750 rpm. A thermocouple (7) and a manometer (6) were positioned upstream the power turbine.

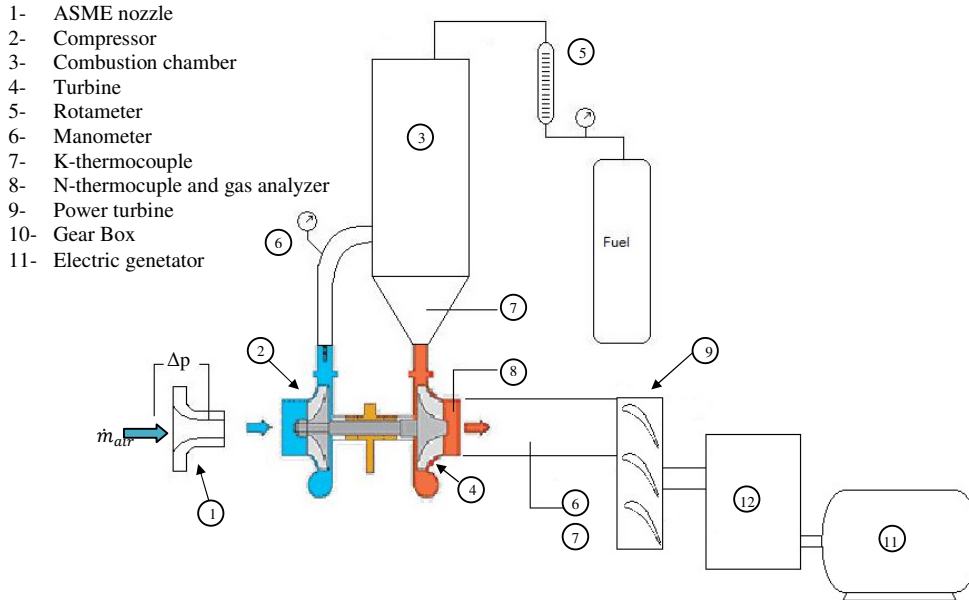


Figure 1. Experimental test rig

Table 1 summarizes some basic data that were obtained from experimental runs.

Table 1. Experimental Data

	Value
Air flow rate (kg/s)	0,17
LPG flow rate (kg/s)	0.0030
Combustion chamber exit temperature (K)	702
Pressure in the chamber (bar gauge)	1.0
Temperature upstream of the power turbine (K)	795

### 3. COMBUSTION CHAMBER DESIGN

The development of combustion chambers for such gas turbines remains as a critical issue, on account of emissions as well as temperature homogeneity. In Tuccillo et al (2005) and Cameretti (2007), a comprehensive report of combustion chambers of micro gas turbines is given. Tuccillo et al conducted a literature review on combustors modeling using both, experimental and numerical tools. They have numerically studied three combustors concepts: diffusion annular, lean pre-mixed and Rich burn-Quick quench-Lean burn, where the flame stabilization is achieved by a swirler.

The main dimensions of the proposed combustion chamber are given in Table 2. The geometry of the chamber is shown in Figure 2. The flame was stabilized by a bluff body mounted at the head of the liner. The option for a bluff body reflects manufacturing issues, although the authors are aware of the advantages of swirlers on flame stabilization.

The fuel was injected at the centre of the bluff body through a radial injector with four holes of 2.0 mm diameter. There were four rows of secondary air, of 8.0 mm diameter each. Additionally, there was one row of dilution holes of 12 mm diameter placed just above the air inlet, after the compressor. The ignition was provided by a spark plug located at the internal surface of the bluff body.

Table 2. Main dimension of combustion chamber.

Casing diameter (mm)	152
Casing length (mm)	500
Liner diameter (mm)	127
Liner length (mm)	450
Bluff Body inner diameter (mm)	50
Bluff Body outer diameter (mm)	60
Number of secondary air rows	4
Number and Diameter of the secondary air holes (mm) per row	4x8
Number of the dilution air rows	1
Number and Diameter (mm) of the dilution holes	4x12

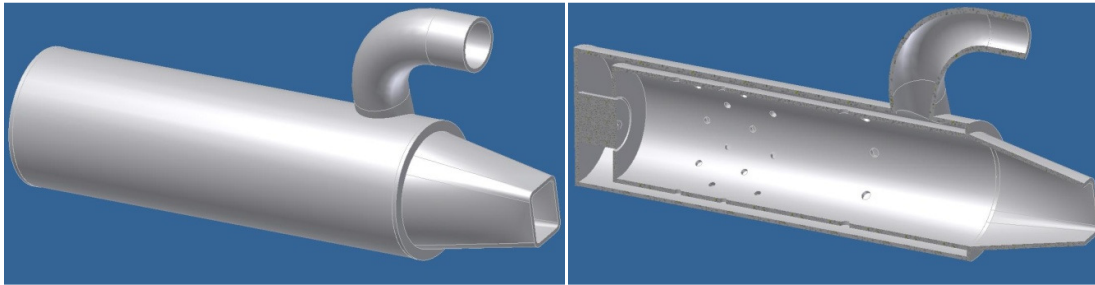


Figure 2. Geometry of combustion chamber

## 2.1 Numerical methods

The turbulent flow inside the combustion chamber was simulated using the commercial CFD code Fluent®, based on finite volume method. In order to account for the turbulent combustion, two models were used RANS and LES. The conservation and transport equations are described in the following.

The mass conservation for the mean flow is given by

$$\frac{\partial \rho}{\partial t} + \text{div}(\rho \cdot \vec{u}) \quad (1)$$

where  $\rho$  is the density of the mixture,  $t$  is the time and  $\vec{u}$  is the mean velocity vector.

The momentum conservation equation applied to a fluid control volume leads to the averaged momentum equation:

$$\frac{\partial}{\partial t}(\rho u_i) + \frac{\partial}{\partial x_j}(\rho u_i u_j) = -\frac{\partial p}{\partial x_i} + \frac{\partial}{\partial x_j} \left[ \mu \left( \frac{\partial u_i}{\partial x_j} + \frac{\partial u_j}{\partial x_i} - \frac{2}{3} \delta_{ij} \frac{\partial u_l}{\partial x_l} \right) \right] + \frac{\partial}{\partial x_j}(-\rho \overline{u'_i u'_j}) \quad (2)$$

where  $p$  is the static pressure and  $\rho \overline{u'_i u'_j}$  is the Reynolds stresses tensor in the RANS approach .

### 2.1.1 The Reynold Stress Model

In the Reynolds Stress Model the tensor  $\overline{\rho u'_i u'_j}$  is calculated by solving transport equations for each of its components, Veerstedt et al (2007). The transport equation of the Reynolds stress tensor,  $R_{ij}$ , is given by:

$$\frac{DR_{ij}}{Dt} = \frac{\partial R_{ij}}{\partial t} + C_{ij} = P_{ij} + D_{ij} - \varepsilon_{ij} + \Pi_{ij} + \Omega_{ij} \quad (3)$$

In the Equation (3) the terms of convection,  $C_{ij}$ , production,  $P_{ij}$ , production due rotating frame,  $\Omega_{ij}$ , do not need modelling. The remaining terms need modelling. The diffusion term,  $D_{ij}$ , is modelled as:

$$D_{T,ij} = \frac{\partial}{\partial x_k} \left( \frac{\mu_t}{\sigma_k} \frac{\partial \overline{u'_i u'_j}}{\partial x_k} \right) \quad (4)$$

where,  $\mu_t$  is the turbulent viscosity, defined in Equation 5. The value of 0.82 is used for the turbulent Prandtl number,  $\sigma_k$  .

$$\mu_t = \rho C_\mu \frac{k^2}{\varepsilon} \quad (5)$$

The standard value of  $C_\mu$  is 0.09.

The dissipation rate,  $\varepsilon_{ij}$ , is modelled with the assumption of isotropy of small dissipative eddies. The modelling is done in such a way that this term affects only normal Reynolds stresses ( $i=j$ ) and in equal magnitude. Then,

$$\varepsilon_{ij} = \frac{2}{3} \varepsilon \delta_{ij} \quad (6)$$

In Equation (6),  $\varepsilon$  is the dissipation rate of turbulent kinetic energy and  $\delta_{ij}$  is the Kronecker delta.

The pressure-strain term  $\Pi_{ij}$  in the RSM model is decomposed in three components as:

$$\Pi_{ij} = \Pi_{ij,1} + \Pi_{ij,2} + \Pi_{ij,w} \quad (7)$$

where,  $\Pi_{ij,1}$  is known as return-to-isotropy,  $\Pi_{ij,2}$  is called rapid pressure-stain and  $\Pi_{ij,w}$  is the wall-reflection. The linear pressure-strain model was used in the present work.

In order to avoid refining the grid at the solid boundaries, standard wall functions were used.

### 2.1.2 Thermochemistry model

The thermochemistry model is based on the conserved scalar model, Turns (1996). In this model, the mixture fraction, Turns (1996) and Veerstedt et al (2007), is the variable transported. Due its definition, the transport equation for the mean mixture fraction,  $f$ , does not have source term and reads

$$\frac{\partial}{\partial t} (\rho f) + \frac{\partial}{\partial x_j} (\rho f u_j) = \frac{\partial}{\partial x_j} \left( \rho D_f \frac{\partial f}{\partial x_j} \right) \quad (8)$$

Under the assumption of unit Lewis number for an adiabatic system, the normalized equation for the mixture enthalpy has the same structure and boundaries conditions as the mixture fraction. Therefore in the conserved scalar model only one transport equation for the scalar  $f$  was solved, representing the thermochemical variables, the mixture fraction and the mixture enthalpy. In this model, the temperature distribution is directly related to the mixture fraction field inside the combustor.

### 2.1.3 Boundary conditions

The boundaries conditions for velocities used in the simulations are given in the Table 3. All external walls and the liner were considered adiabatic. The mixture fraction is 1.0 at the fuel inlet and zero at the air inlet.

Table 3. Velocities Boundaries Conditions

Variable	Prescribed value	Length Scale [m] and Turbulence Intensity [-]
Air inlet	0.17 kg/s	0.015; 10%
Outlet	Developed flow	-
Fuel inlet	0.0033 kg/s for LPG	0.0025; 10%

### 2.1.4 Numerical results

In this section the results of the simulations are shown and compared to experimental data, if available. The results for the simulation of LPG fuel is shown in the Figures 3 to 5. The RANS simulated velocity field in the mid plane of the computational domain, near to the fuel injection, is shown in Figure 2

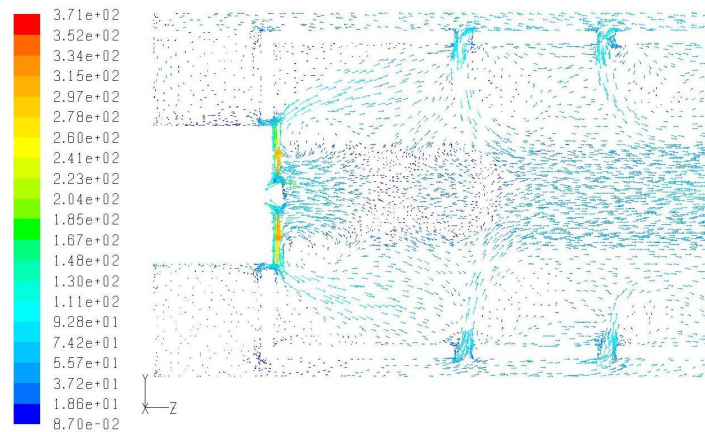


Figure 3. RANS Velocity [m/s] field in the combustor mid plane near the fuel injector

The gas recirculation behind the bluff body can be seen in Figure 4. This recirculation zone is established not only due to presence of the bluff body, but also due to the secondary air holes, as shown in Figure 4. The recirculation zone behind the bluff body is able to stabilize the flame. The stability of the flame can be observed during power up phase of the micro gas turbine. At start up phase, the flame reaches the exit of the power turbine as a consequence of reduced air flow rate provide by the compressor. As the compressor rpm and the mass flow rates increase, the flame is no longer visible at the power turbine exit. It means that the stabilization is working properly. Therefore, one can conclude the bluff body is working properly, as far as the stabilization of the flame is concerned.

The temperature distribution inside the liner and casing is shown in the Figure 3. It is important to emphasize that heat conduction through the liner was not accounted for in our predictions. Therefore, pre-heating of the air in the liner/casing annuli was not accurately predicted. The turbulence model predicts higher temperatures along the liner walls. This is probably due the mixing process produced by the bluff body. Furthermore, it can be seen temperature level of about 1600 K just upstream of the dilution holes, meaning that the flame extends from the fuel injector until the dilution holes. One can see that there are temperature gradients at the outlet plane ranging from 960K to 1120K. It is worthy of note that the higher temperatures were found near to the wall of the liner, an undesirable feature. The mean gas temperature measured after the combustor, with K-type thermocouple, was of about 702K. Since the thermocouple was placed at the centre of the outlet plane the measured temperature value may not be representative of the whole outlet plane. This observation was confirmed by the numerical predictions, which showed non-homogeneity temperature in that plane. From the comparison between numerical and experimental data, one can conclude that the numerical simulation should at least take into account the heat losses – external convection and radiation – in order to better predict the outlet combustion chamber temperature.

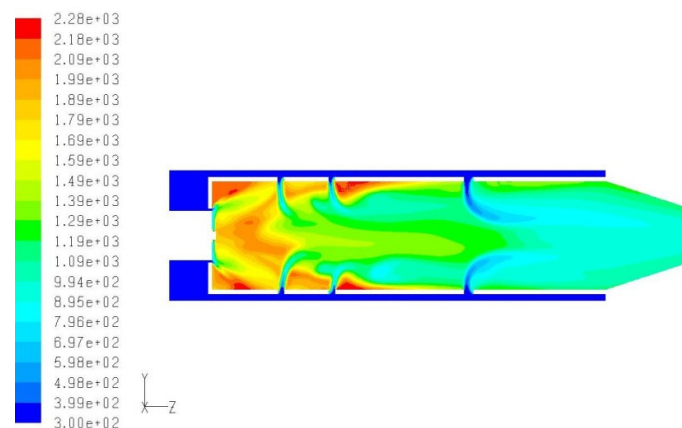


Figure 4. RANS Mean Temperature [K] field in the combustion chamber

Mixture fraction distribution can be used to infer the flame structure inside the liner. Figure 4 shows the values of mixture fraction for the RANS simulations. The plots show that just downstream of the secondary air holes there are spots of mixture fraction of about 0.03. It means that the mixture processes between fuel and oxidizer is still going on. This may explain the high temperatures observed at the combustion chamber outlet.

The thermochemistry model used in the present work was based on chemical equilibrium, meaning that a mixture of fuel/air always reacts until chemical equilibrium, despite of the mixing characteristic time scale. One can see spots of temperature, just downstream the secondary air holes, which corresponds to stoichiometric mixture fraction. Ideally, downstream of the secondary air holes, the mixture fraction should be near stoichiometry or even locally lean. It is known that the chemistry equilibrium approach is not able to account for such strong turbulence chemistry interaction. However, one should be aware of the occurrence of flame instabilities.

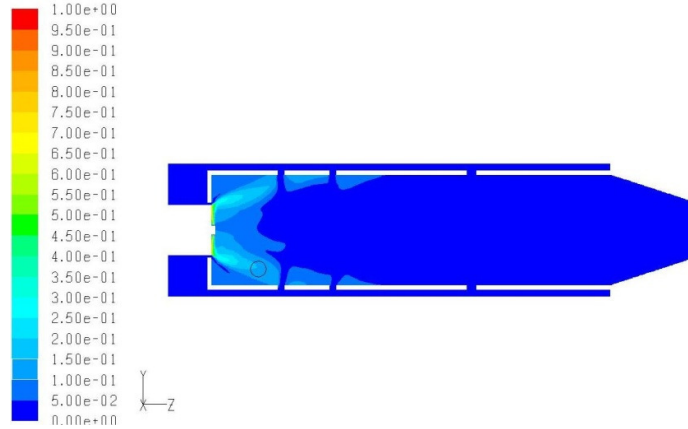


Figure 5. RANS Mean Mixture Fraction field in the combustion chamber

The experimental data measured during the gas generator operation are resumed in Table 3.

Table 4. Experimental Data

	LPG
Air flow rate (kg/s)	0,17
LPG flow rate (kg/s)	0.0030
Combustion chamber exit temperature (K)	702
Pressure in the chamber (bar gauge)	1.0
CO mole fraction downstream the HP turbine (ppm)	63
O2 mole fraction downstream the HP turbine	0.165
Temperature downstream of the turbine (K)	795

The global equivalence ratio, estimated with the measured fuel and air flow rates, was 0.25. This equivalence ratio corresponds to an adiabatic flame temperature of 965K for the LGP fuel, which is slightly above that measured at the exit of the high pressure (HP) turbine. As it is shown in Table 3, the CO content at the gas generator exit is very low.

#### 4. BASIC DESIGN OF POWER TURBINE

The design of the power turbine was carried with some preliminary data that were taken from basic project data. A 1-D meanline methodology was used to obtain the velocity triangles. This basis design follows the theory presented by Cohen et al and Wilson et al. For the sake of manufacturing simplicity, an axial turbine was the primary choice, though the low mass flux could point to a radial in-flow type turbomachinery. To comply with this, a partial admission axial turbine was designed. Figure 6 presents a cross section of an axial turbine, with number 1, 2 and 3 defining the design stations.

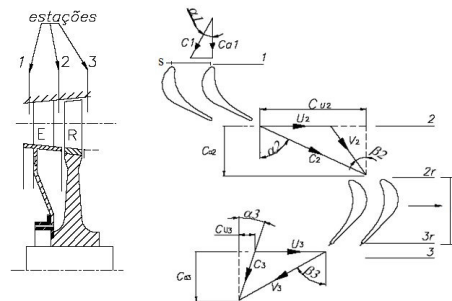


Figure 6. Axial turbine

The 1-D meanline approach makes the assumption that the gas properties taken from the blade mean plane are valid for the whole blade height. In other words, there is neither pressure nor temperature gradients in the radial direction. Besides exhaust gas properties, some other dimensional constraints were applied in the initial design stage. These data are summarized in Table 5.

Table 5. Power turbine initial dimensions

Mean radius ( $R_m$ )	0.067 m
Blade height (h)	0.03 m
Chord (c)	0.02
Pitch (s)	0.6c
Speed	15.000 rpm

Following the stations presented in Figure 6, Table 6 presents the thermodynamic properties used in the axial turbine design. The exhaust gas was assumed to be composed mainly by air in the first design loop, which was modeled as ideal gas.

Table 6. Thermodynamic properties.

P1	1.2 bar
T1	700 °C
P3	1 bar
Mass flow	0.17 kg/s

Other assumptions were also considered in the first design phase: isentropic efficiency of 80%, no losses due to tip leakage or secondary flows. Applying proposed methodology, the velocity triangles were established. Figure 7 presents the usual representation of such results. Table 7 presents the angle results, chord, pitch and number of blades, n, considering partial admission.

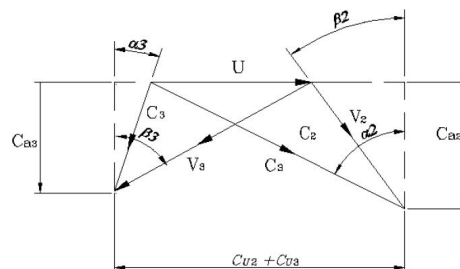


Figure 7. Velocity triangles

Table 7. Project results

$\alpha_1$	0°	$\beta_1$	0°
$\alpha_2$	70°	$\beta_2$	71.4°
$\alpha_3$	60°	$\beta_3$	56.2°
s – stator	13.6 mm	s – rotor	11.4 mm
c – stator	22.6 mm	c – rotor	19.0 mm
n – stator	15	n – rotor	37

These data were used to construct the blade profile, which is present in figure 8. The program “Blade Design”, from Steam Turbine Pro, was used.



Figure 8. Stator and rotor profiles, respectively.

## 5. RESULTS AND CONCLUSIONS

The rotor designed in the section 4 was manufactured and assembled with the gas generator of the micro gas turbine. Measurements indicate speed of 12000rpm, net power of 1,5 kW. The net power was measured at the electric generator output. The thermal efficiency for the micro gas turbine can be defined as

$$\eta = \dot{W}_{liq} / \dot{Q}_{in}, \quad (9)$$

where  $\dot{W}_{liq}$  is the net power output, measured at the electric generator and  $\dot{Q}_{in}$  is the heat power input, which is calculated based on the Low Heating Value (LHV) of LPG as follow:

$$\dot{Q}_{in} = \dot{m}_{fuel} LHV$$

Performing the calculation with the measured data for fuel consumption and using LHV=46.357kJ/kg, one obtains a global thermal efficiency of 1%. This very low thermal efficiency can be partially explained by the very low pressure ratio (1,8) at the compressor and very low isentropic efficiencies of the compressor, gas generator turbine and power turbine. The thermal efficiency of an ideal Brayton cycle, for the pressure ratio of 1,8 would be about 15%.

## 5. ACKNOWLEDGEMENTS

This project is supported by FAPESP under the grant 2007/03072-1 and ANP-PRH-19. The authors would like to thank the support from BorgWarner Turbo Systems and Bernauer Ventiladores.

## 6. REFERENCES

- Cameretti, M.C., Reale, F. and Tuccillo, R., 2007, Cycle Optimization and Combustion Analysis in a Low-NOx Micro Gas Turbine, Journal of Engineering for Gas Turbines and Power – Transactions of the ASME, Vol 129 pp. 994-1003,
- Cohen, H., Saravanamuttoo, 1972, “Gas turbine theory”, Longman Group UK Limited, 5<sup>th</sup> ed. 512p.
- MLA, 15 July 2009, Fluent User’s Guide, 2009, <http://www.fluentusers.com/fluent/doc/ori/html/ug>
- Tuccillo, R., Cameretti, M. C., 2005, Combustors and Combustion for MGT applications, Micro Gas Turbines, pp 5-1-5-56, Educations Notes RTO-EN-AVT131, paper 5
- Turns, S.R., 2007, “An introduction to combustion: concepts and applications”, McGraw-Hill, 1996, 704p.
- Versteeg, H.K., Malalasekera, W, 2007 “An introduction to computational fluid dynamics – the finite volume method”, 2nd edition, Prentice Hall, London, UK.,
- Wilson, D.G., Korakiantis, T., 1998, “The design of high-efficiency turbomachinery and gas turbines”, Prentice Hall, 2<sup>nd</sup> ed, 593p.

## 5. RESPONSIBILITY NOTICE

The authors are the only responsible for the printed material included in this paper.